SPACECRAFT LOCALIZATION VIA ANGLE MEASUREMENTS FOR AUTONOMOUS NAVIGATION IN DEEP SPACE MISSIONS

Nicola Ceccarelli [*] **Andrea Garulli** [**]
Antonio Giannitrapani [**] **Mirko Leomanni** [**]
Fabrizio Scortecci [***]

[*] *Air Force Research Laboratory, AFRL/VACA*
[**] *Dipartimento di Ingegneria dell'Informazione, Università di Siena, Via Roma 56, Siena, Italy*
[***] *AEROSPAZIO Tecnologie s.r.l. Rapolano Terme, Siena, Italy*

Abstract: This paper deals with spacecraft autonomous navigation in deep space missions. The considered problem is that of spacecraft localization based on angular measurements. The dynamic model of the spacecraft accounts for several perturbing effects, such as Earth and Moon gravitational field asymmetry and errors associated with the Moon ephemerides. The measurement process is based on elevation and azimuth of Moon and Earth with respect to the spacecraft reference system. Distance measurements are not employed. Position and velocity of the spacecraft are estimated by using both the Extended Kalman Filter (EKF) and the Unscented Kalman Filter (UKF). The performance of the filters are evaluated on an example of Earth-to-Moon transfer mission.

1. INTRODUCTION

Following the successful SMART-1 mission of the European Space Agency (ESA, 2003; Milligan *et al.*, 2005), a growing interest in lunar and outer planetary explorations performed by small and cheap spacecrafts propelled by electric propulsion systems is emerged in the space community. It is a fact that the propulsive efficiency of an electrically driven spacecraft allows to perform planetary exploration with a minimum propellant consumption when compared to traditional chemical propulsion systems. The reduced mass of the spacecraft permits the use of smaller and cheaper launchers or even to share the launch cost by installing the spacecraft as a piggy-back of larger missions. However, the low thrust produced by an electric propulsion system leads to a continuous thrusting strategy which, in turn, requires an accurate knowledge of the spacecraft position and attitude during the transfer orbit. This aspect will substantially increase the cost of the ground segment. Therefore, autonomous navigation becomes a fundamental requirement for this type of missions.

Localization of spacecrafts is usually very accurate when GPS range measurements are available. The problem becomes more challenging when GPS signals are not available, like in high-Earth orbits or in long range missions, such as Earth-to-Moon transfers. In these cases, spacecraft navigation is often handled by ground-based tracking stations, thus making it unfeasible for low-cost spacecraft missions. In order to make spacecrafts fully autonomous, it is necessary to devise self-localization and navigation algorithms relying only on measurements provided by on-board sensors (see e.g. (Tuckness and Young, 1995; Long *et al.*, 2000)).

In this paper, the problem of spacecraft self-localization is addressed using angular measurements. First, a dynamic model of the spacecraft is formulated, which takes into account several perturbing effects such as Earth and Moon gravitational field asymmetry and errors associated with the Moon ephemerides. It is assumed that the navigation system is able to estimate the spacecraft attitude (e.g., by using a star tracker sensor), and the spacecraft is equipped with sensors providing measurements of elevation and azimuth of Moon and Earth with respect to the spacecraft reference system. Range measurements, which are often difficult to obtain or not sufficiently reliable, are not required. Then, position and velocity of the spacecraft are estimated by employing both the classical Extended Kalman Filter (EKF) and the Unscented Kalman Filter (UKF) (see e.g. (Crassidis and Junkins, 2004)). The filters have been tested on simulated data concerning an example of lunar transfer mission, and the results have been compared with those provided by an accurate mission simulator. Two different types of sensors, with different accuracy levels, have been considered. The size of the obtained localization errors, and the associated confidence intervals, show that the proposed algorithms provide reli-

able estimates, whose precision is sufficiently accurate for autonomous navigation of spacecrafts in the considered class of missions.

2. SPACECRAFT MODEL

The following dynamic model for the spacecraft is considered

$$\ddot{\mathbf{r}} = -\frac{\mu}{\rho^3}\mathbf{r} + \mu_{\leftmoon}\left(\frac{\mathbf{r}_{s\leftmoon}}{\rho_{s\leftmoon}^3} - \frac{\mathbf{r}_{\leftmoon}}{\rho_{\leftmoon}^3}\right) + \mathbf{u}, \qquad (1)$$

where $\mathbf{r} = [x, y, z]$, $\mathbf{r}_{\leftmoon} = [x_{\leftmoon}, y_{\leftmoon}, z_{\leftmoon}]$ are respectively the spacecraft and Moon positions in the Earth Centered Inertial reference system (ECI (M. D. Griffin, 2004)), see Figure 1. In equation (1), $\mu = 398600.4415\ km^3/s^2$ and $\mu_{\leftmoon} = 4902.801\ km^3/s^2$ are the gravitational parameters; $\rho = \|\mathbf{r}\|$, $\rho_{\leftmoon} = \|\mathbf{r}_{\leftmoon}\|$ are respectively the distances of the spacecraft and the Moon from the earth; $\mathbf{r}_{s\leftmoon} = \mathbf{r}_{\leftmoon} - \mathbf{r}$ is the moon position with respect to the spacecraft, and $\rho_{s\leftmoon} = \|\mathbf{r}_{s\leftmoon}\|$. The input $\mathbf{u}$ is the acceleration provided by the propulsion system. If we denote the thrust vector and its norm by $\mathbf{T}$ and T respectively, then the input is $\mathbf{u} = \frac{\mathbf{T}}{m}$, where m is the spacecraft mass, evolving as $\dot{m} = -\frac{T}{I_{sp}\cdot g}$, and I_{sp} is the specific impulse (see (M. D. Griffin, 2004)).

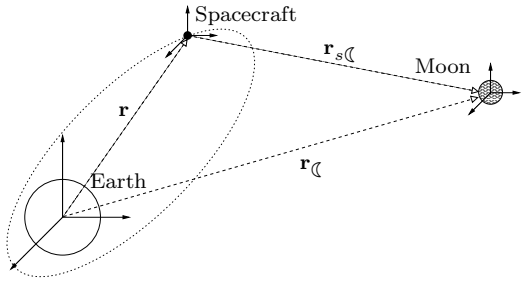

Fig. 1. The ECI reference system

Although model (1) takes into account the most relevant gravitational terms, there are several possible sources of model errors deriving from perturbing effects, such as Earth and Moon gravitational field asymmetry, air drag, sun attraction, and errors associated with the Moon ephemerides (King-Hele, 1987). According to Cowell's formulation, process disturbances are modelled by an additive term $\boldsymbol{\xi}$ in the right hand side of (1). We consider an error term given by:

$$\boldsymbol{\xi} = \boldsymbol{\omega}_{\earth} + \boldsymbol{\omega}_{\leftmoon} + \boldsymbol{\omega}_t. \qquad (2)$$

The terms $\boldsymbol{\omega}_{\earth}$ and $\boldsymbol{\omega}_{\leftmoon}$ represent the disturbances associated with the Earth and Moon gravitational field asymmetries. These disturbances are modelled as Gaussian noises. The standard deviation of $\boldsymbol{\omega}_{\earth}$ has been estimated by evaluating the difference between the gravitational force predicted by the nominal model $\frac{\mu}{\rho^3}\mathbf{r}$ and the one yielded by the Earth gravitational model JGM-2 (ECSS, 2000). For each fixed value of ρ, the empirical standard deviation has been computed at 900 different spacecraft positions, uniformly distributed on a sphere of radius ρ centered at the Earth. In Fig. 2(a) the standard deviation along each coordinate has been reported as a function of ρ. The behavior can be approximated by the model $\boldsymbol{\omega}_{\earth} = \mathbf{G}_{\earth}\boldsymbol{\omega}_e$, where $\mathbf{G}_{\earth} = \mathrm{diag}\left(\left[\frac{1.68\cdot10^{10}}{\rho^4}, \frac{1.68\cdot10^{10}}{\rho^4}, \frac{2.71\cdot10^{10}}{\rho^4}\right]\right)$ and $\boldsymbol{\omega}_e \in \mathbb{R}^3$ is an independent white noise with standard normal distribution $\mathcal{N}(0, I)$. The same has been done for the Moon by considering the model LP-150 (Konopliv *et al.*, 2001). The standard deviations of the modelled disturbance as a function of $\rho_{s\leftmoon}$, reported in Fig. 2(b), can be approximated by $\boldsymbol{\omega}_{\leftmoon} = \mathbf{G}_{\leftmoon}\,\boldsymbol{\omega}_m$, where $\mathbf{G}_{\leftmoon} = \frac{10^9}{\rho_{s\leftmoon}^4} I$ and $\boldsymbol{\omega}_m \in \mathbb{R}^3$ is an independent white noise with distribution $\mathcal{N}(0, I)$.

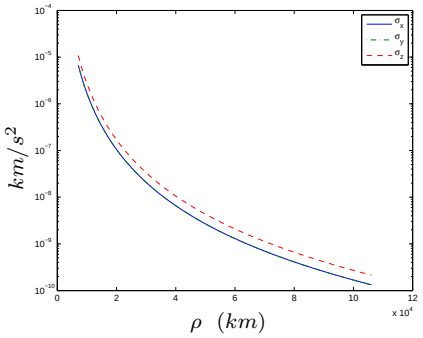

(a) Earth

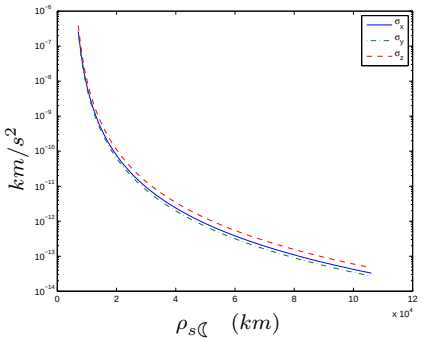

(b) Moon

Fig. 2. Standard deviations associated with Earth and Moon gravitational field asymmetries

The last term $\boldsymbol{\omega}_t$ in (2), is a white noise with zero mean and covariance $\sigma_t^2 I$, which takes into account unmodelled effects such as sun attraction, radiation pressure, dragging, integration errors. The variance σ_t^2 will play the role of a tuning knob in the design of the filters.

It is also assumed that the propulsion system generates a perturbed thrust $\hat{\mathbf{T}} = (1+\omega_u)\mathbf{T}$, with ω_u white noise distributed as $\mathcal{N}(0, \sigma_u^2)$. Hence the resulting perturbed input is $\hat{\mathbf{u}} = (1+\omega_u)\mathbf{u}$. Notice that the thrust perturbation affects also the fuel mass evolution.

Another error source is due to the fact that the Moon position is not known exactly. The Moon

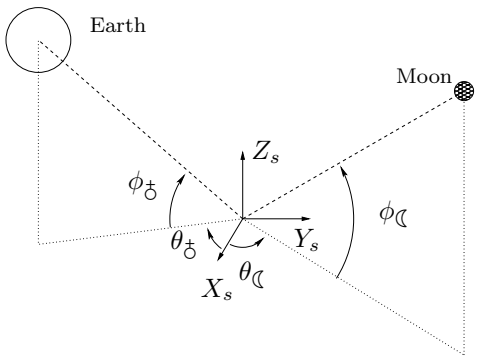

Fig. 3. Angle measurements in the spacecraft reference system

ephemerides algorithm (Vallado, 2001) has been used to estimate the Moon position. Hence, the Moon position is affected by the error vector $\mathbf{e}_{\mathbb{C}} = [\epsilon_{x\mathbb{C}}, \epsilon_{y\mathbb{C}}, \epsilon_{z\mathbb{C}}]'$, where each component is an independent noise signal distributed as $\mathcal{N}(0, \sigma^2_{\epsilon_{\mathbb{C}}})$, with $\sigma_{\epsilon_{\mathbb{C}}} = 10\ km$ (Seidelmann *et al.*, 1985). Therefore, if $\hat{\mathbf{r}}_{\mathbb{C}}$ is the Moon position provided by the ephemerides, one has

$$\hat{\mathbf{r}}_{\mathbb{C}} = \mathbf{r}_{\mathbb{C}} + \mathbf{e}_{\mathbb{C}}\ . \tag{3}$$

By including all the perturbation terms and error sources into the nominal model (1), one obtains the perturbed dynamic model

$$\ddot{\mathbf{r}} = -\frac{\mu}{\rho^3}\mathbf{r} + \mu_{\mathbb{C}}\left(\frac{\hat{\mathbf{r}}_{\mathbb{C}} - \mathbf{e}_{\mathbb{C}} - \mathbf{r}}{\|\hat{\mathbf{r}}_{\mathbb{C}} - \mathbf{e}_{\mathbb{C}} - \mathbf{r}\|^3} - \frac{\hat{\mathbf{r}}_{\mathbb{C}} - \mathbf{e}_{\mathbb{C}}}{\|\hat{\mathbf{r}}_{\mathbb{C}} - \mathbf{e}_{\mathbb{C}}\|^3}\right) + (1+\omega_u)\mathbf{u} + \mathbf{G}_{\leftmoon}\boldsymbol{\omega}_e + \mathbf{G}_{\mathbb{C}}\,\boldsymbol{\omega}_m + \boldsymbol{\omega}_t. \tag{4}$$

Similarly, the perturbed spacecraft mass evolution is given by

$$\dot{m} = -(1+\omega_u)\frac{T}{I_{sp}\cdot g}. \tag{5}$$

The spacecraft is equipped with sensors that provide angular measurements of azimuth and elevation of Moon and Earth, with respect to a local reference system centered at the spacecraft and aligned to ECI, see Fig. 3 (recall that it is assumed that the attitude of the spacecraft is known). Hence, by taking into account (3), the measurements equations are given by

$$\theta_{\leftmoon} = \text{atan}_2(-y, -x) + v_{\theta_{\leftmoon}} \tag{6}$$

$$\phi_{\leftmoon} = \text{atan}\left(\frac{-z}{\sqrt{x^2+y^2}}\right) + v_{\phi_{\leftmoon}} \tag{7}$$

$$\theta_{\mathbb{C}} = \text{atan}_2\left(\hat{y}_{\mathbb{C}} - \epsilon_{y\mathbb{C}} - y, \hat{x}_{\mathbb{C}} - \epsilon_{x\mathbb{C}} - x\right) + v_{\theta_{\mathbb{C}}} \tag{8}$$

$$\phi_{\mathbb{C}} = \text{atan}\left(\frac{\hat{z}_{\mathbb{C}} - \epsilon_{z\mathbb{C}} - z}{\sqrt{(\hat{x}_{\mathbb{C}} - \epsilon_{x\mathbb{C}} - x)^2 + (\hat{y}_{\mathbb{C}} - \epsilon_{y\mathbb{C}} - y)^2}}\right) + v_{\phi_{\mathbb{C}}} \tag{9}$$

where $v_{\theta_{\leftmoon}}$, $v_{\phi_{\leftmoon}}$, $v_{\theta_{\mathbb{C}}}$ and $v_{\phi_{\mathbb{C}}}$ are independent disturbances with distribution $\mathcal{N}(0, \sigma_v^2)$.

3. STATE ESTIMATION

In order to tackle the spacecraft localization problem via off-the-shelf estimation algorithms, it is convenient to rewrite the dynamic model (4)-(5) and the measurement equations (6)-(9) in a more compact form. To this purpose let us introduce the state vector $\mathbf{X} = [x, y, z, \dot{x}, \dot{y}, \dot{z}, m]'$ containing the spacecraft position and velocity, as well as its mass. If we stack all the uncertainty sources of the dynamic model in a disturbance vector $\mathbf{w} = [\boldsymbol{\omega}'_e\ \boldsymbol{\omega}'_m\ \boldsymbol{\omega}'_t\ \omega_u\ \mathbf{e}'_{\mathbb{C}}]'$, then the time evolution of the state vector can be written as

$$\dot{\mathbf{X}} = f(\mathbf{X}, \mathbf{u}, \mathbf{w}, t), \tag{10}$$

with $f(\cdot,\cdot,\cdot,\cdot)$ defined according to (4)-(5). Similarly, if the errors affecting the measurements are grouped as $\mathbf{v} = [v_{\theta_{\leftmoon}}\ v_{\phi_{\leftmoon}}\ v_{\theta_{\mathbb{C}}}\ v_{\phi_{\mathbb{C}}}\ \mathbf{e}'_{\mathbb{C}}]'$, the measurement equations (6)-(9) can be cast as

$$\mathbf{Y} = h(\mathbf{X}, \mathbf{v}, t), \tag{11}$$

where $\mathbf{Y} = [\theta_{\leftmoon}\ \phi_{\leftmoon}\ \theta_{\mathbb{C}}\ \phi_{\mathbb{C}}]'$. Notice that the explicit dependence of the functions $f(\cdot,\cdot,\cdot,\cdot)$ and $h(\cdot,\cdot,\cdot)$ on time t is due to the presence of the predicted Moon position $\hat{\mathbf{r}}_{\mathbb{C}}(t)$ in the expressions (4) and (8)-(9). Actually, $\hat{\mathbf{r}}_{\mathbb{C}}(t)$ can be thought of as a known time-varying parameter or a given input. A further step towards the implementation of recursive state estimation algorithms is the discretization of equation (10). Let us denote by ΔT the sampling time. Then a discrete-time version of equation (10) is given by

$$\begin{aligned}&\mathbf{X}((k+1)\Delta T) = \mathbf{X}(k\Delta T)\\ &+\Delta T f(\mathbf{X}(k\Delta T), \mathbf{u}(k\Delta T), \mathbf{w}(k\Delta T), k\Delta T)\\ &\triangleq f_d(\mathbf{X}(k\Delta T), \mathbf{u}(k\Delta T), \mathbf{w}(k\Delta T), k\Delta T)).\end{aligned}$$

In the following, for ease of notation, we will get rid of the dependence on the sampling time ΔT and will refer to the discrete-time model

$$\begin{aligned}\mathbf{X}(k+1) &= f_d(\mathbf{X}(k), \mathbf{u}(k), \mathbf{w}(k), k)\\ \mathbf{Y}(k) &= h(\mathbf{X}(k), \mathbf{v}(k), k).\end{aligned} \tag{12}$$

The estimation of the spacecraft position and velocity boils down to a state estimation problem for system (12). In this work, two different estimators are considered: the Extended Kalman Filter (EKF) and the Unscented Kalman Filter (UKF).

3.1 *Extended Kalman Filter*

The EKF is a classic recursive state estimator for nonlinear systems. Hereafter, the EKF equations are reported for model (12). Let us denote the covariance matrix of the process disturbance by $Q = E\{\mathbf{w}\mathbf{w}'\}$ and that of the measurement noise by $R = E\{\mathbf{v}\mathbf{v}'\}$. Notice that the error $\mathbf{e}_{\mathbb{C}}$ affects both the dynamic model and the measurement equation, i.e. it is included both in $\mathbf{w}$ and in $\mathbf{v}$. To account for the correlation between $\mathbf{w}$ and $\mathbf{v}$ let us denote their cross-covariance matrix by $S = E\{\mathbf{w}\mathbf{v}'\} = \begin{bmatrix} 0_{10\times 4} & 0_{10\times 3} \\ 0_{3\times 4} & S_{\mathbf{e}} \end{bmatrix}$ with $S_{\mathbf{e}} = E\{\mathbf{e}_{\mathbb{C}}\,\mathbf{e}'_{\mathbb{C}}\}$. Finally, let $\hat{\mathbf{X}}_k^+$ be the state estimate at time k and let P_k^+ be the estimation error covariance matrix

at the same time. Then, the EKF prediction and correction equations are as follows (Crassidis and Junkins, 2004).

Prediction

$$\hat{\mathbf{X}}_{k+1}^{-} = f_d(\hat{\mathbf{X}}_k^{+}, \mathbf{u}_k, \mathbf{0}, k)$$
$$P_{k+1}^{-} = F_k P_k^{+} F_k' + G_k Q G_k'$$

Correction

$$\begin{aligned}
\hat{\mathbf{X}}_{k+1}^{+} &= \hat{\mathbf{X}}_{k+1}^{-} + K_{k+1}[\mathbf{Y}_{k+1} - h(\hat{\mathbf{X}}_{k+1}^{-}, \mathbf{0}, k+1)] \\
P_{k+1}^{+} &= [I - K_{k+1}H_{k+1}]P_{k+1}^{-} \\
&\quad -K_{k+1}V_{k+1}S'G_k' \\
K_{k+1} &= [P_{k+1}^{-}H_{k+1}' + G_k S V_{k+1}'] \\
&\quad [H_{k+1}P_{k+1}^{-}H_{k+1}' + V_{k+1}RV_{k+1}' \\
&\quad +H_{k+1}G_k S V_{k+1}' + V_{k+1}S'G_k'H_{k+1}']^{-1}
\end{aligned}$$

where the superscript "-" denotes the prediction of the corresponding quantity before the measurement at time $k+1$ is taken, and

$$F_k \triangleq \left.\frac{\partial f_d}{\partial \mathbf{X}}\right|_{\hat{\mathbf{X}}_k^{+}, \mathbf{u}_k, \mathbf{0}}, \quad G_k \triangleq \left.\frac{\partial f_d}{\partial \mathbf{w}}\right|_{\hat{\mathbf{X}}_k^{+}, \mathbf{u}_k, \mathbf{0}},$$
$$H_k \triangleq \left.\frac{\partial h}{\partial \mathbf{X}}\right|_{\hat{\mathbf{X}}_k^{-}, \mathbf{0}}, \qquad V_k \triangleq \left.\frac{\partial h}{\partial \mathbf{v}}\right|_{\hat{\mathbf{X}}_k^{-}, \mathbf{0}}.$$

Clearly, if the measurements are available with a frequency lower than the sampling one (e.g., every $N\Delta T$), then the intermediate state estimates are updated according only to the prediction step (i.e., N prediction steps are performed between two consecutive correction steps).

3.2 *Unscented Kalman Filter*

The UKF is a recursive state estimator based on the Unscented Transform, which is a method to approximate the mean and covariance of a random variable undergoing a nonlinear transformation (Julier and Uhlmann, 1997; Wan and van der Merwe, 2001). The underlying idea is to estimate the statistics of the transformed variable from a set of $2n+1$ points (called *sigma points*), with n being the dimension of the considered random variable. Sigma points are generated deterministically, on the basis of the (known) covariance matrix of the initial random variable and depending on the parameters of the filter. Unlike the EKF, the UKF does not require the evaluation of the Jacobians, since the gains to be used during the estimation are computed directly from the sigma points. In the following the UKF update equations are reported for the dynamic model (12) (Wan and van der Merwe, 2001). Let us define the augmented state vector $\mathbf{X}^a = [\mathbf{X}'\ \mathbf{w}'\ \mathbf{v}']' \in \mathbb{R}^L$. Denote by $\hat{\mathbf{X}}_k^a$ and P_k^a the state estimate and the corresponding error covariance matrix

$$\hat{\mathbf{X}}_k^a = [(\hat{\mathbf{X}}_k^{+})'\ \mathbf{0}\ \mathbf{0}]' \qquad P_k^a = \begin{bmatrix} P_k^{+} & 0 & 0 \\ 0 & Q & S \\ 0 & S' & R \end{bmatrix}$$

Sigma-point generation. For $i = 0, \ldots, 2L$:

$$\begin{aligned}
\boldsymbol{\chi}_{i,k}^a &= \begin{cases} \hat{\mathbf{X}}_k^a & i = 0 \\ \hat{\mathbf{X}}_k^a + \left(\sqrt{(L+\lambda)P_k^a}\right)_i & i = 1, \ldots, L \\ \hat{\mathbf{X}}_k^a - \left(\sqrt{(L+\lambda)P_k^a}\right)_{i-L} & i = L+1, \ldots, 2L \end{cases} \\
&\triangleq [(\boldsymbol{\chi}_{i,k}^x)'\ (\boldsymbol{\chi}_{i,k}^w)'\ (\boldsymbol{\chi}_{i,k}^v)']'
\end{aligned}$$

where $(P)_i$ denotes the i-th column of matrix P.

Prediction

$$\begin{aligned}
\boldsymbol{\chi}_{i,k+1|k}^x &= f_d(\boldsymbol{\chi}_{i,k}^x, \mathbf{u}_k, \boldsymbol{\chi}_{i,k}^{\boldsymbol{w}}, k) \qquad i = 0, \ldots, 2L \\
\hat{\mathbf{X}}_{k+1}^{-} &= \sum_{i=0}^{2L} W_i^{(m)} \boldsymbol{\chi}_{i,k+1|k}^x \\
P_{k+1}^{-} &= \sum_{i=0}^{2L} W_i^{(c)} [\boldsymbol{\chi}_{i,k+1|k}^x - \hat{\mathbf{X}}_{k+1}^{-}][\boldsymbol{\chi}_{i,k+1|k}^x - \hat{\mathbf{X}}_{k+1}^{-}]' \\
\boldsymbol{\mathcal{Y}}_{i,k+1|k} &= h(\boldsymbol{\chi}_{i,k+1|k}^x, \boldsymbol{\chi}_{i,k}^{\boldsymbol{v}}, k+1) \qquad i = 0, \ldots, 2L \\
\hat{\mathbf{Y}}_{k+1}^{-} &= \sum_{i=0}^{2L} W_i^{(m)} \boldsymbol{\mathcal{Y}}_{i,k+1|k}
\end{aligned}$$

Correction

$$\begin{aligned}
P_{YY} &= \sum_{i=0}^{2L} W_i^{(c)} [\boldsymbol{\mathcal{Y}}_{i,k+1|k} - \hat{\mathbf{Y}}_{k+1}^{-}][\boldsymbol{\mathcal{Y}}_{i,k+1|k} - \hat{\mathbf{Y}}_{k+1}^{-}]' \\
P_{XY} &= \sum_{i=0}^{2L} W_i^{(c)} [\boldsymbol{\chi}_{i,k+1|k}^x - \hat{\mathbf{X}}_{k+1}^{-}][\boldsymbol{\mathcal{Y}}_{i,k+1|k} - \hat{\mathbf{Y}}_{k+1}^{-}]' \\
\hat{\mathbf{X}}_{k+1}^{+} &= \hat{\mathbf{X}}_{k+1}^{-} + P_{XY}P_{YY}^{-1}(\mathbf{Y}_{k+1} - \hat{\mathbf{Y}}_{k+1}^{-}) \\
P_{k+1}^{+} &= P_{k+1}^{-} - P_{XY}P_{YY}^{-1}P_{XY}'
\end{aligned}$$

The weights $W_i^{(\cdot)}$ are computed as follows

$$\begin{aligned}
W_0^{(m)} &= \frac{\lambda}{L+\lambda}, \quad W_0^{(c)} = \frac{\lambda}{L+\lambda}(1 - \alpha^2 + \beta), \\
W_i^{(m)} &= W_i^{(c)} = \frac{1}{2(L+\lambda)}, \quad i = 1, \ldots, 2L
\end{aligned}$$

where $\lambda = \alpha^2(L+\kappa) - L$, and α, β and κ are the tuning parameters of the filter.

4. SIMULATION RESULTS

In this section, the performance of the filters is analyzed by simulating an example of Earth-to-Moon transfer mission, with initial eccentricity $e = 0.5$, inclination $i = 10^o$, altitude perigee $a = 3{\cdot}10^4 Km$. The forcing input is a continuous thrust tangential to the trajectory, with $\mathbf{T} = T\frac{\dot{\mathbf{r}}}{\|\dot{\mathbf{r}}\|}$, and $T = 50mN$. The filters have been tested for 70 days of mission. The sampling time used to discretize the dynamic model (10) is $\Delta T = 15\ s$, whereas the angular measurements (11) are supposed to be available once per hour. This means that both filters perform a correction step every 240 prediction steps. The standard deviations of $\boldsymbol{\omega}_e$, $\boldsymbol{\omega}_m$ and $\mathbf{e}_{\mathbb{Q}}$ have been chosen as pointed out in section 2, that of ω_u is $\sigma_u = 0.01$, while σ_t acts as a tuning parameter of the filters.

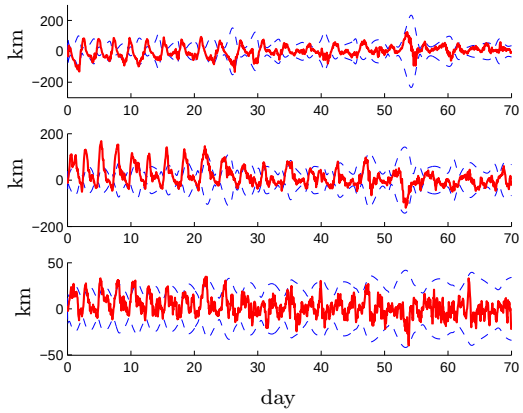

(a) Sensor A

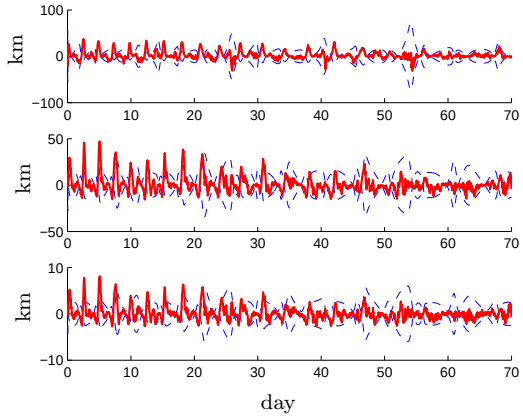

(b) Sensor B

Fig. 4. EKF: x, y, z estimation errors (solid) and 99% confidence intervals (dashed).

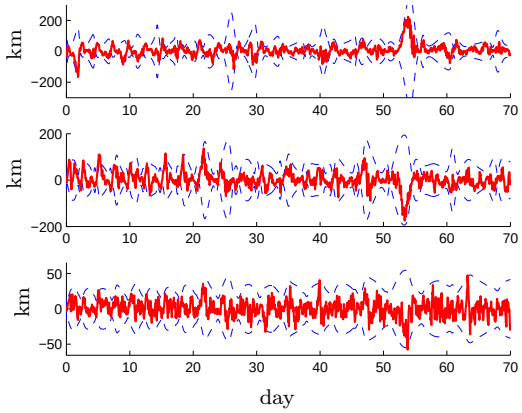

(a) Sensor A

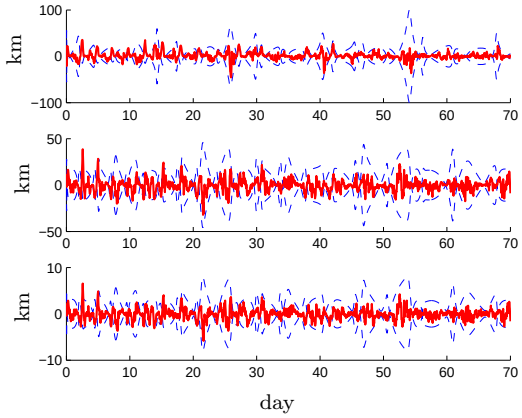

(b) Sensor B

Fig. 5. UKF: x, y, z estimation errors (solid) and 99% confidence intervals (dashed).

Although sensor modelling is not an issue addressed in this work, two different kinds of possible devices have been considered: a sensor based on standard vision system technology (hereafter sensor A) and a star tracker sensor (sensor B). The standard deviation of the measurement errors is assumed to be $\sigma_v = 0.01\frac{\pi}{180}$ for sensor A, and $\sigma_v = 10^{-4}\frac{\pi}{180}$ for sensor B.

The filters have been initialized with $\hat{\mathbf{X}}_0^+ = \mathbf{X}(0)$ and $P_0^+ = \text{diag}\left(\left[1, 1, 1, 10^{-4}, 10^{-4}, 10^{-4}, 10^{-6}\right]\right)$. For each filter both the estimation errors and the corresponding standard deviations are evaluated by comparing the state estimates to the output of an accurate mission simulator, jointly developed by Aerospazio Tecnologie s.r.l. and the Dipartimento di Ingegneria dell'Informazione of the Università di Siena.

For the EKF, the standard deviation of the process disturbance ω_t has been tuned to $\sigma_t = 10^{-5}$. Smaller values of σ_t resulted in a significant lack of consistency of the filter (estimation errors remarkably outside the 99% confidence intervals). Figure 4 shows the EKF estimation errors for coordinates x, y, z, and the corresponding 99% confidence intervals, for sensors A and B. In Table 1 the sample standard deviation of the estimation errors are reported (results are averaged over 10 simulation runs). The overall average localization error turns out to be 48.82 km for sensor A, and 9.33 km for sensor B.

	sensor A	sensor B
x	36.80 km	8.75 km
y	42.55 km	9.53 km
z	10.81 km	1.66 km
$\dot{x}$	$1.33 \cdot 10^{-3} km/s$	$4.00 \cdot 10^{-4} km/s$
$\dot{y}$	$1.51 \cdot 10^{-3} km/s$	$5.78 \cdot 10^{-4} km/s$
$\dot{z}$	$3.43 \cdot 10^{-4} km/s$	$1.18 \cdot 10^{-4} km/s$

Table 1. EKF: sample standard deviation of estimation errors.

For the UKF, the following parameters have been used for the generation of the *sigma* points: $\alpha = 10^{-3}$, $\kappa = 0$, $\beta = 2$. The standard deviation of the process disturbance ω_t has been tuned to $\sigma_t = 10^{-7}$. In Figure 5 the x, y, z estimation errors and the 99%, confidence intervals are shown for sensors A and B. Table 2 reports the sample standard deviation of the estimation errors, averaged over 10 simulation runs. The overall average localization error is now 38.00 km for sensor A and 8.02 km for sensor B. Hence, with respect to the EKF the localization error has been reduced of about 20% in the former case, and about 15% in the latter. Moreover, Figures 4 and 5 show

that UKF features better consistency properties (error almost always inside the 99% confidence intervals). It is worth remarking that these results have been obtained with a smaller value of σ_t with respect to the EKF.

	sensor A	sensor B
x	31.59 km	8.07 km
y	31.57 km	7.09 km
z	10.94 km	1.26 km
$\dot{x}$	$1.07 \cdot 10^{-3} km/s$	$4.27 \cdot 10^{-4} km/s$
$\dot{y}$	$1.18 \cdot 10^{-3} km/s$	$5.08 \cdot 10^{-4} km/s$
$\dot{z}$	$4.48 \cdot 10^{-4} km/s$	$1.44 \cdot 10^{-4} km/s$

Table 2. UKF: sample standard deviation of estimation errors.

Figures 4-5 show a periodic behavior of the position estimation errors. Intuition suggests that the peaks are relative to configurations in which Earth, Moon and the spacecraft are aligned. This is confirmed by Fig. 6, where the mean square localization error (MSE) is plotted against the alignment angle. The figure refers to the UKF with sensor B, but a similar phenomenon occurs in the other settings. The error peaks are mostly grouped around angles zero (Moon and Earth aligned on opposite side respect to the spacecraft) and $\pm\pi$ (Moon and Earth aligned on the same side respect to the spacecraft) Conversely, the lowest values correspond to angles close to $\pm\frac{\pi}{2}$.

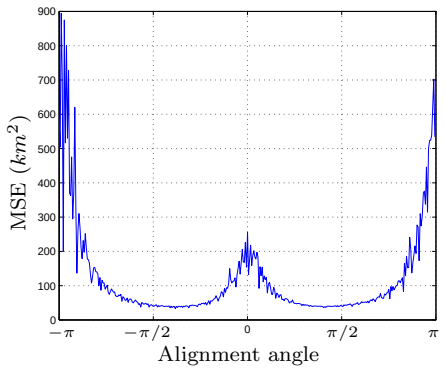

Fig. 6. Mean square error of position estimation vs. spacecraft-Earth-Moon alignment

5. CONCLUSIONS AND FUTURE WORK

A preliminary investigation on the performance of recursive estimation techniques for autonomous navigation of low-cost deep space missions has been presented. The localization procedure is based only on angular measurements of celestial bodies with respect to the spacecraft reference system, and does not require range measurements which are often difficult to obtain. Both filters considered in the paper, EKF and UKF, provide localization errors which are reasonably small for the considered type of missions. Although both techniques resulted in the same order of errors, the UKF has shown better performance in terms of average localization precision and consistency of the estimates. Moreover, the tuning of the UKF has led to smaller values of the process disturbance covariance with respect to the EKF.
The ongoing work concerns different topics. The dynamic model should be enriched in order to consider eclipse effects. Sun azimuth and elevation measurements will be added to improve the localization precision. The development of accurate sensor models for the measurement process and the integration of an attitude estimation procedure in the autonomous navigation module are further issues to be addressed.

6. REFERENCES

Crassidis, J.L. and J.L. Junkins (2004). *Optimal Estimation of Dynamic Systems*. Applied mathematics and nonlinear science series. Chapman & Hall/CRC.

European Cooperation for Space Standardization (2000). Space engineering.

European Space Agency (2003). http://www.esa.int/specials/smart-1.

Julier, S. J. and J. K. Uhlmann (1997). A new extension of the Kalman filter for nonlinear systems. In: *Proc. of AeroSense: The 11th Int. Symp. on Aerospace/Defence Sensing, Simulation and Controls*. pp. 182–193.

King-Hele, D.G. (1987). *Satellite Orbits in an Atmosphere: Theory and Applications*. Springer.

Konopliv, A.S., S.W. Asmar, E. Carranza, W.L. Sjogren and D.N. Yuan (2001). Recent gravity models as a result of the lunar prospector mission. *Icarus* **150**, 1–18.

Long, A. C., D. Leung, D. Folta and C. Gramling (2000). Autonomous navigation of high-Earth satellites using celestial objects and doppler measurements. In: *AIAA/AAS Astrodynamics Specialist Conference*. Denver, CO.

M. D. Griffin, J. R. French. (2004). *Space Vehicle Design*. AIAA education. 2nd ed.. AIAA.

Milligan, D., D. Gestal, P. Pardo-Voss, O. Camino, D. Estublier and C. Koppel (2005). SMART-1 electric propulsion operational experience.. In: *Proc. of the 29th Int. Electric Propulsion Conf.*. Princeton, NJ.

Seidelmann, P.K., E.J. Santoro and K.F. Pulkkinen (1985). Systematic differences between planetary observations and ephemerides. In: *Second U. S. Hungary Workshop*. Dynamical Astronomy. Univ. of Texas Press. pp. 55–65.

Tuckness, D.G. and S.Y. Young (1995). Autonomous navigation for lunar transfer. *Journal of Spacecraft and Rockets*. pp. 279-285.

Vallado, A. (2001). *Fundamentals of Astrodynamics and Applications*. 2nd ed.. Microcosm/Kluwer.

Wan, E. and R. van der Merwe (2001). The Unscented Kalman Filter. In: *Kalman Filtering and Neural Networks* (S. Haykin, Ed.). Chap. 7, pp. 221–280. Wiley.